The current issue and full text archive of this journal is available at
www.emeraldinsight.com/0961-5539.htm

Numerical study of heat transfer and pressure drop for flow past inline and staggered tube bundles

S. Jayavel and Shaligram Tiwari
Department of Mechanical Engineering, Indian Institute of Technology Madras, Chennai, India

Received 10 June 2008
Revised 9 November 2008
Accepted 5 December 2008

Abstract

Purpose – The purpose of this paper is to develop an indigenous three-dimensional computational code and apply it to compare flow and heat transfer characteristics for inline and staggered arrangement of circular tubes in a tube bundle.

Design/methodology/approach – A finite-volume based computational code is developed to solve the momentum and energy equations for flow through a three-dimensional rectangular channel and past built-in tube bundles having inline and staggered arrangement. The approach is based on SIMPLE algorithm. The basic conservation equations of mass, momentum and energy are solved over a body-fitting grid on the physical domain to obtain the flow and temperature fields.

Findings – Heat transfer and pressure drop are compared for inline and staggered tube arrangements in a tube bundle over range of Reynolds numbers $300 \leq \mathrm{Re} \leq 800$. Results are validated suitably against those available in literature.

Research implications – Tube-fin heat exchangers with continuous fins on a tube array are commonly used in air-conditioning industry and in air-cooled condensers of power plants. The flow structure within the finned tube bank is complex due to the presence of a circular tube, which causes flow acceleration over the fin surface and flow separation on the back side of the tube resulting in low velocity wake region. The present study provides a better understanding of flow behavior and heat transfer for inline and staggered arrangement of tube bundles in tube-fin heat exchangers at different Reynolds numbers.

Originality/value – A numerical code based on finite volume method has been developed and used for computations to predict heat transfer and pressure drop characteristics for flow past inline and staggered arrangement of circular tubes. Predictions are made from the computed results about suitability of staggered/inline tube arrangements in a given range of Reynolds number.

Keywords Heat exchangers, Flow, Numerical analysis, Heat transfer, Pressure
Paper type Research paper

Nomenclature

B	channel width ($= l_2$)
D	diameter of circular tube
F	mass flux through a cell face
gf	goodness factor
H	channel height
HTR	heat transfer ratio ($= j_{\mathrm{stag}}/j_{\mathrm{inl}}$)
j	Colburn factor
l	length
Nu	Nusselt number
$\overline{Nu}$	average Nusselt number
n	distance normal to surface
Pr	Prandtl number
PDR	pressure drop ratio ($= \Delta p_{\mathrm{stag}}/\Delta p_{\mathrm{inl}}$
p	pressure
R	radius of circular tube
r	radial coordinate
Re_D	Reynolds number based on tube diameter
S	surface area of cell face
S_ϕ	volumetric source term
T	dimensionless temperature

International Journal of Numerical Methods for Heat & Fluid Flow
Vol. 19 No. 8, 2009
pp. 931-949

0961-5539
DOI 10.1108/09615530910994432

t	time
U	velocity
u	axial velocity component
V	Volume
v	span-wise velocity component
w	velocity component normal to channel wall

Greek

Γ	diffusion coefficient
ϕ	transport property (u, v, w or T)
Θ	non-dimensional temperature
ρ	density
μ	dynamic viscosity
θ	angle measured clockwise from forward stagnation point with respect to tube center
τ	skin friction drag ($\tau = \mu(\partial u/\partial n)$)
ν	kinematic viscosity

Subscripts

1	axial direction
2	span-wise direction
3	direction normal to channel wall
b	bulk
inl	inline
j	cell face index
m	mean
o	overall
stag	staggered
sp	span-averaged
w	wall

1. Introduction

Fin-tube heat exchangers with continuous fins on a tube array are commonly used in air-conditioning industry and in air-cooled condensers of power plants. One of the challenging tasks for researchers is to optimize the arrangement of tube bundles in the fin-tube heat exchangers associated with maximum heat transfer and minimum pressure drop/pumping power. This is primarily because the air side heat transfer coefficient is low and pressure drop associated with flow of air past the tube is normally higher than flow of any liquid coolant. Hence, for large air-cooled condensers, optimization of configurations of tubes in the bundle which would result in reduction of condenser size and also of pumping power is an important need. Gangacharyulu (2001) developed a mathematical model and computer code for heat transfer and pressure drop analysis of cross-flow compact heat exchangers. A numerical study was carried out by Ramezanpour *et al.* (2006) to evaluate optimum arrangement of staggered tube bundle in cross-flow with Reynolds numbers in the range of 1,000-100,000. They employed k-ϵ turbulence model. Khan *et al.* (2006) carried out an analytical study to investigate heat transfer from tube banks in cross-flow under isothermal boundary conditions. They developed models for inline and staggered arrangements of tubes which are applicable for use over a wide range of parameters when determining heat transfer from tube banks. Plane and slit types of fins for tube-fin heat exchangers were investigated by Tony Sheu and Tsai (1999) using finite volume technique. They studied the advantages of fins with perforations and flow complexities.

The experimental results from Herchang *et al.* (2002) showed that the averaged heat transfer coefficient of staggered configuration is 14-32 per cent higher than that of inline configuration, where they performed an experimental study using an infrared thermo-vision to monitor temperature distribution over a plate-fin surface of the heat exchanger. Kim and Kim (2005) tested 22 heat exchangers with a variation of fin pitch,

number of tube rows and tube alignment. They showed that air-side heat transfer coefficient decreases with a reduction of the fin pitch and an increase of the number of tube rows, over the Reynolds number range of 500-900. Wilson and Khalil (2000) investigated the case of two rows of tubes in cross-flow having both inline and staggered arrangements and reported the effects of flow and geometry parameters on the friction factor and local as well as global Nusselt number. The effect of number of transverse rows in tube bundles on heat transfer and pressure drop for staggered finned-tube bundles was studied experimentally by Kwak *et al.* (2003). Beal and Spalding (1999) presented numerical calculations for transient flow past inline and staggered arrangement of circular tubes, in the Reynolds number range of 30-3,000. They showed that for the inline arrangement where each tube is in the shadow of the previous one, the effect of flow on downstream tubes in terms heat transfer from their surfaces is less pronounced. Rich (1973) proposed a correlation for Colburn-factor (j) in terms of Reynolds number which was arrived from experimental results on tube-fin heat exchangers. A three-dimensional numerical study on the flow and heat transfer characteristics in a narrow rectangular duct with a built-in circular tube in cross-flow has been carried out by Tiwari *et al.* (2003). They reported that in the Reynolds number range from 600 to 1,400, onset of turbulence does not take place due to effect of narrow channel walls.

Although a substantial amount of experimentation and numerical predictions have been reported in literature, the present work aims at investigation of the performance of tube bundles in tube-fin heat exchangers for inline and staggered arrangement of tubes and comparison of heat transfer and pressure drop characteristics for both the arrangements. The study also compares the effect of Reynolds number ($300 \leq \mathrm{Re} \leq 800$) on heat transfer and pressure drop for inline and staggered arrangement of tube bundles. The numerical predictions have been made using higher order schemes for discretization of convective fluxes.

2. Problem statement

Figures 1(a) and (b) show the computational domains for inline and staggered arrangements of circular tubes in a tube bundle. The domains have been considered with specified dimensions. All the length dimensions are non-dimensionalized with respect to tube diameter (D) and velocities with respect to mean flow velocity at inlet. The circular tubes are cross-confined and built-in with a rectangular channel of length (l_1) $= 11.5D$, width (l_2) $= 4.0D$ and height (l_3) $= 1.0D$. The distance between centers of the two tubes in the flow direction is kept fixed as $5D$. In staggered arrangement, the spanwise separation between the two tubes is maintained as $4D$. The blockage ratio ($= D/l_2$) is 0.25. The channel walls and tube surfaces are maintained at a constant temperature. The flow Reynolds number has been defined as, $\mathrm{Re}_D = U_m D/\nu$. Air is the working fluid for which the Prandtl number is fixed as $\mathrm{Pr} = 0.7$.

3. Governing equations and boundary conditions

The present work considers Reynolds number $\mathrm{Re}_D = 600$ for flow of air for which assumptions of incompressible flow remain valid. Moreover, the fluid properties are assumed to remain constant. The incompressible three-dimensional Navier-Stokes and the energy equations can be represented in the general convection-diffusion source integral form of the following equation for a control volume, V.

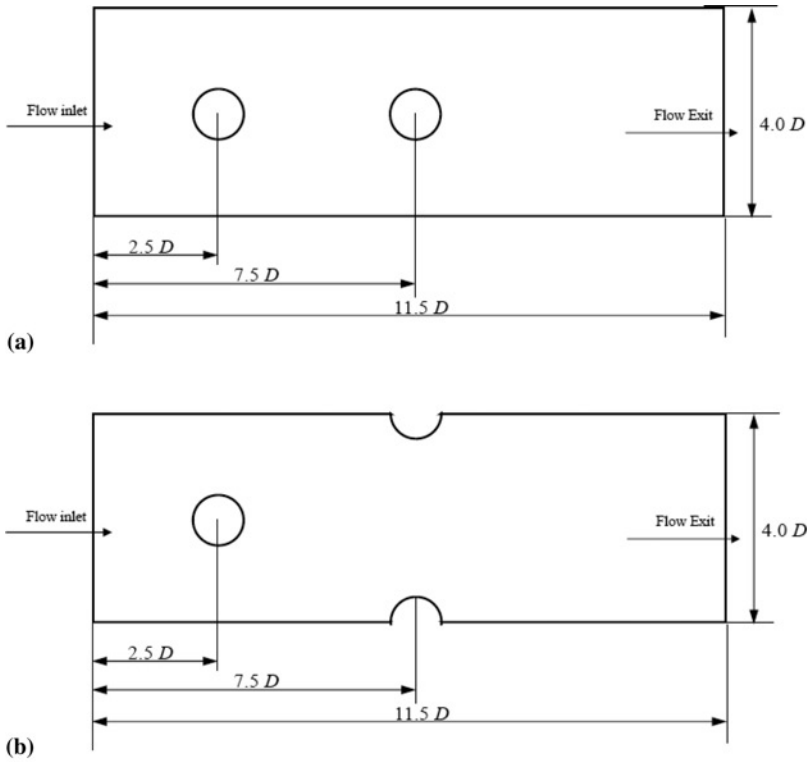

Figure 1.
Two-dimensional schematic representation of the computational domain

Notes: (a) Inline arrangement of tubes and (b) staggered arrangement of tubes

$$\frac{\partial}{\partial t}\int_V \rho\phi\, dV + \int_S [\rho\vec{u}\Phi - \Gamma_\phi \nabla\phi]\cdot d\vec{S} = \int_V S_\phi\, dV \tag{1}$$

where ϕ represents a transport property (u, v, w or T). The general equation can represent continuity, momentum and energy equations for values of the variables given in Table I.

The equation of motion and energy equation require appropriate boundary conditions for the completeness of the model. The boundaries of the computational domain are divided into four types, namely, inlet, exit, symmetrical side-walls and solid surfaces. Appropriate boundary conditions of no-slip for top and bottom walls and for tube surfaces, symmetry for side-walls, inflow at the inlet and convective outflow or Orlanski (1976) type at the exit have been used. The boundary conditions for the given computational domain are summarized in Table II.

	ϕ	Γ_ϕ	S_ϕ
Continuity	1	0	0
Momentum	u, v, w	μ	$\frac{\partial p}{\partial x}, \frac{\partial p}{\partial y}, \frac{\partial p}{\partial z}$
Energy	T	k/C_p	0

Table I.
Variables for general transport equation

4. Grid generation

The grid employed for computations is structured grid of body-fitting type, as shown schematically in Figure. 2, generated using transfinite interpolation method and smoothened by partial differential equaiton (PDE) method. It is basically a two-dimensional grid in X-Y plane which is stacked uniformly in the Z-direction. The geometrical quantities for each control volume, such as volume, the outward facing unit normal vector and the area of each face of the control volume have been computed for each grid cell.

A thorough grid-independence has been confirmed considering variation of span-averaged Nusselt number along length of the channel as shown in Figure 3, for three different grid-sizes of $203 \times 63 \times 19, 213 \times 73 \times 21$ and $233 \times 83 \times 23$. The maximum deviation in results is found to be within 4 per cent. All the computations in the present study correspond to a grid-size of $233 \times 83 \times 23$.

Top and bottom walls $u = v = w = 0, \frac{\partial p}{\partial z} = 0$ and $T = T_w$
Side-walls $\frac{\partial u}{\partial y} = \frac{\partial w}{\partial y} = 0, v = 0, \frac{\partial p}{\partial y} = 0$, and $\frac{\partial T}{\partial y} = 0$
Inlet to the channel $u = U_\infty, v = w = 0, \frac{\partial p}{\partial x} = 0$ and $T = T_\infty$
Channel exit; $\frac{\partial \phi}{\partial t} + U_{av}\frac{\partial \phi}{\partial x} = 0$ (Orlanski, 1976)
Obstacle surface; $u = v = w = 0, \frac{\partial p}{\partial n} = 0$ and $T = T_w$, where n denotes normal to the surface

Table II.
Summary of boundary conditions

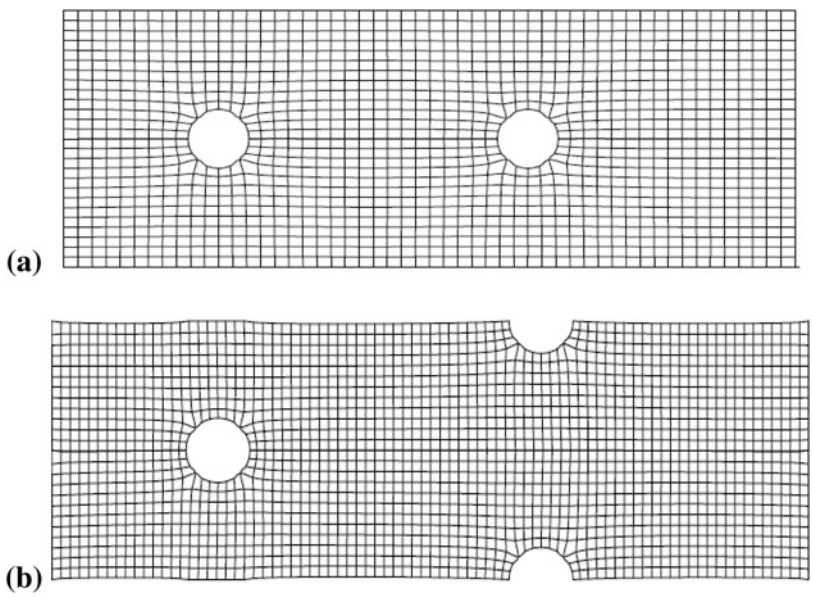

Notes: (a) Inline arrangement of tubes and (b) staggered arrangement of tubes

Figure 2.
Two-dimensional schematic representation of the body-fitted grid employed for computations

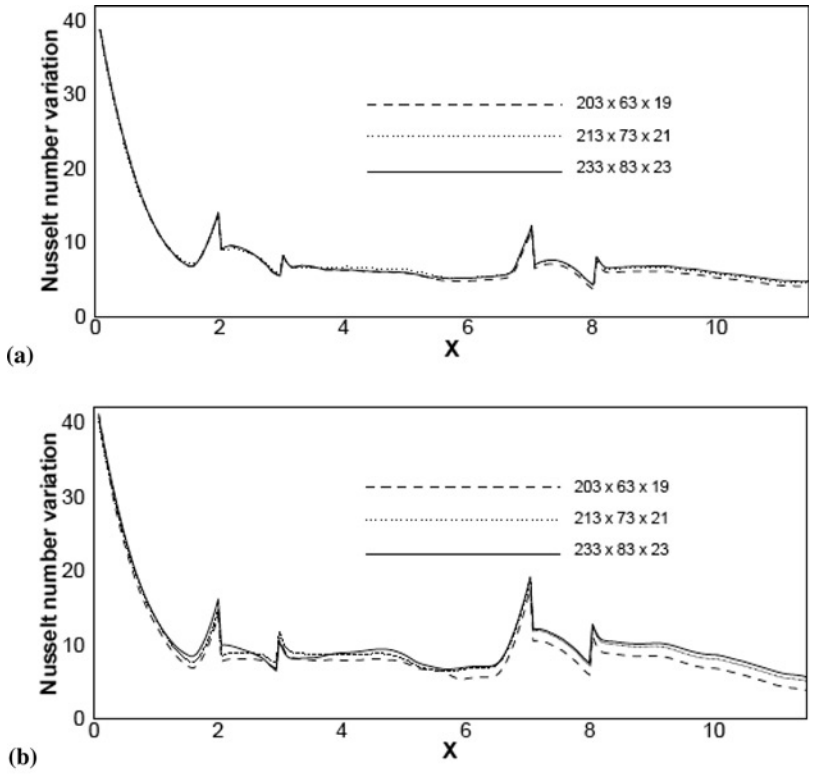

Figure 3.
Grid-independence test for span-averaged Nusselt number variation along length of channel near the bottom wall for (a) inline and (b) staggered arrangement of tubes

Note: Re = 600

5. Solution methodology

The semi-implicit method for pressure linked equations (SIMPLE) algorithm of Patankar (1980) has been used to develop the finite-volume-based computer code. A cyclic series of guess and correct operations have been performed through which, the velocity components are first calculated from the momentum equations using guessed pressure field. The pressure and velocities are then corrected, so as to satisfy continuity equation/mass conservation. The procedure is repeated until convergence of the solution. Furthermore, an improved version of SIMPLER algorithm for numerical simulations of incompressible fluid flow and heat transfer problems capable of enhancing the convergence rate of the iterative solution procedure has been studied by Liu *et al.* (2005).

5.1 Discretization of the convective fluxes

The surface integral over convection flux of variable ϕ is approximated in the following form

$$\int_s \rho \mathrm{u}\phi \cdot \mathrm{dS} \approx \sum_j \rho \phi_j (\mathrm{u.S})_j = \sum_j F_j \phi_j \tag{2}$$

where F_j is the mass flux through face j and ϕ_j is the value of ϕ at the centre of face j. Commonly used techniques in the computation of convective fluxes are second-order

upwind and QUICK (Quadratic Upstream Interpolation for Convective Kinematics) scheme. In the present study QUICK scheme of Leonard (1979) has been employed. It is a velocity-directional-independent interpolation scheme, where three-point upstream-weighted quadratic interpolations for cell face values are used. The QUICK differencing scheme offers higher order accuracy than the central differencing scheme and retains the upwind weighted characteristics as well.

5.2 Discretization of the diffusion fluxes

The diffusion flux consists of two distinct parts, viz normal diffusion and cross-derivative diffusion. The second part arises from the non-orthogonality of the grid. The normal derivative diffusion flux of ϕ through any cell face involves the value of ϕ at cell centers, whereas the cross-derivative diffusion flux takes into account the edge center values of ϕ. In the present study, the normal derivative diffusion flux has been treated implicitly and is coupled with the implicit part of the convective flux to calculate the main coefficients of the discretized equations while the cross-derivative diffusion flux is treated explicitly to avoid the possibility of producing negative coefficients in an implicit treatment. This term together with explicit part of convective flux is added to the source term. The diffusion flux of variable ϕ through the cell faces are evaluated by considering contributions from cross-derivative diffusion alone by using Equation (3). Since the grid employed has been maintained close to orthogonal, the contributions appearing from cross-derivative diffusion fluxes are expected to be quite small and have been ignored. Consequently, the diffusion flux of the transport property ϕ through faces of a computational cell may be written as

$$\int_s \Gamma_\phi \nabla\phi \cdot \mathrm{dS} \approx \sum_j (\Gamma_\phi \nabla\phi \cdot \mathrm{S})_j = \sum_j - F_j^d \tag{3}$$

where F_j represents the diffusion flux associated with face j of the computational cell.

6. Results and discussion

Flow field and heat transfer characteristics for inline and staggered arrangement of tube bundles has been studied over a range of Reynolds number, $300 \leq \mathrm{Re} \leq 800$. Results are presented in terms of flow and temperature fields, temperature and velocity profiles, pressure drop and span-averaged Nusselt number near the bottom wall along length of the channel.

6.1 Flow and heat transfer

Figures 4(a) and (b) present the streamline plots near bottom wall of the channel corresponding to time-averaged field for inline and staggered arrangement of tubes, respectively. The wake regions behind the tubes have poor transport properties due to which the flow and heat transfer in this region require special attention. In Figure 4(a), the wake region of downstream tube for inline arrangement is observed to be wider relative to that of upstream tube. For staggered arrangement of tubes, the flow acceleration between the half-tubes reduces the width of wake region behind upstream tube and in addition is expected to improve heat transfer from the surfaces of the half-tubes.

6.1.1 Axial velocity profiles. Figures 5(a)-(d) show the u-velocity profiles in the X-Y mid-plane and X-Z mid-plane for the inline and staggered arrangements of tubes at various X-locations. The u-velocity profiles in the X-Y and X-Z mid-plane for inline arrangement at various X-locations are shown in Figures 5(a) and (b). The nature of

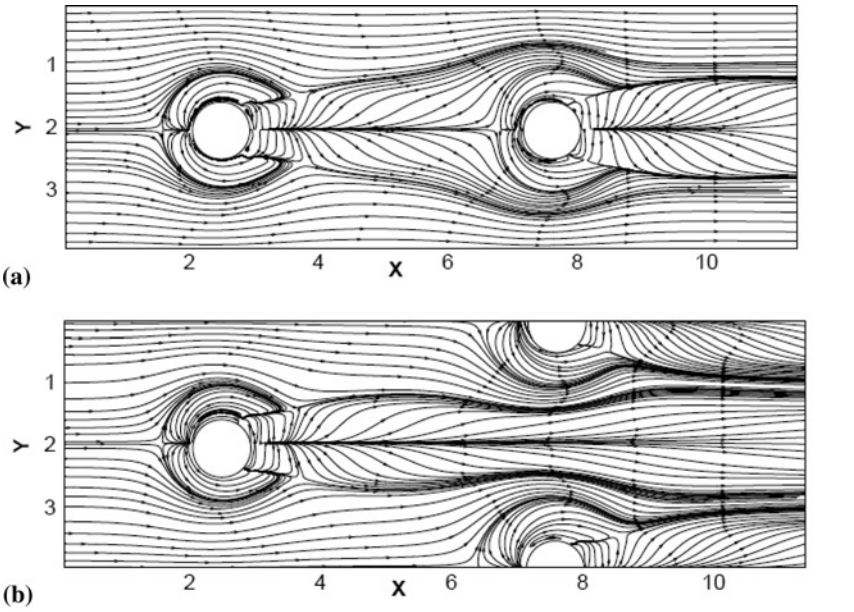

Figure 4.
Streamline plots for time-averaged field near bottom wall of the channel

Notes: (a) Inline arrangement of tubes and (b) staggered arrangement of tubes; Re = 600

velocity profiles in both the planes along length of the channel explain the flow development behavior, e.g. profiles at $X = 4$ and $X = 6$. It is also observed that in the wake of the second tube, the velocity profiles at $X = 10$ and $X = 11$ are steeper near the walls compared to that at $X = 9$. This is because in the aft of the second tube, due to three-dimensionality of the flow, the hydrodynamic boundary layer becomes thinner. Figures 5(c) and (d) present corresponding u-velocity profiles for the staggered arrangement of tubes. In the X-Y plane, at $X = 9$, 10 and 11 the profiles clearly distinguish the accelerated flow that takes place due to the presence of half-tubes in the staggered arrangement. Moreover, in the X-Z plane, the velocity profiles show almost a developed nature in absence of obstructions beyond $X = 9$.

6.1.2 Temperature profiles. Figures 6(a)-(d) show the respective temperature profiles for inline and staggered arrangement of tubes at various X-locations corresponding to the u-velocity profiles shown in Figures 5(a)-(d). The temperature profile varies from the maximum near the wall to its minimum ($T = T_\infty$) in the free stream. In Figures 6(a) and (c), temperature profiles at mid X-Y-plane indicate that the area of hot region is less for staggered arrangement of tubes at $X = 9$, 10 and 11 indicating more heat transfer due to the accelerated flow between half-tubes in staggered arrangement.

Figures 6(b) and (d) show the temperature profiles in the mid X-Z-plane for both the arrangements of tubes. It is observed that from $Z = 0.18$ to $Z = 0.84$ from the bottom wall, the temperature profile remains almost flat and equal to the free stream temperature. The normal distance from the bottom and top heated channel walls at which velocity and temperature attain their maximum and minimum values, respectively, gives information about thicknesses of hydrodynamic and thermal boundary layers, respectively. For air flow, the thermal boundary layer thickness is nearly of the same order as velocity boundary layer thickness.

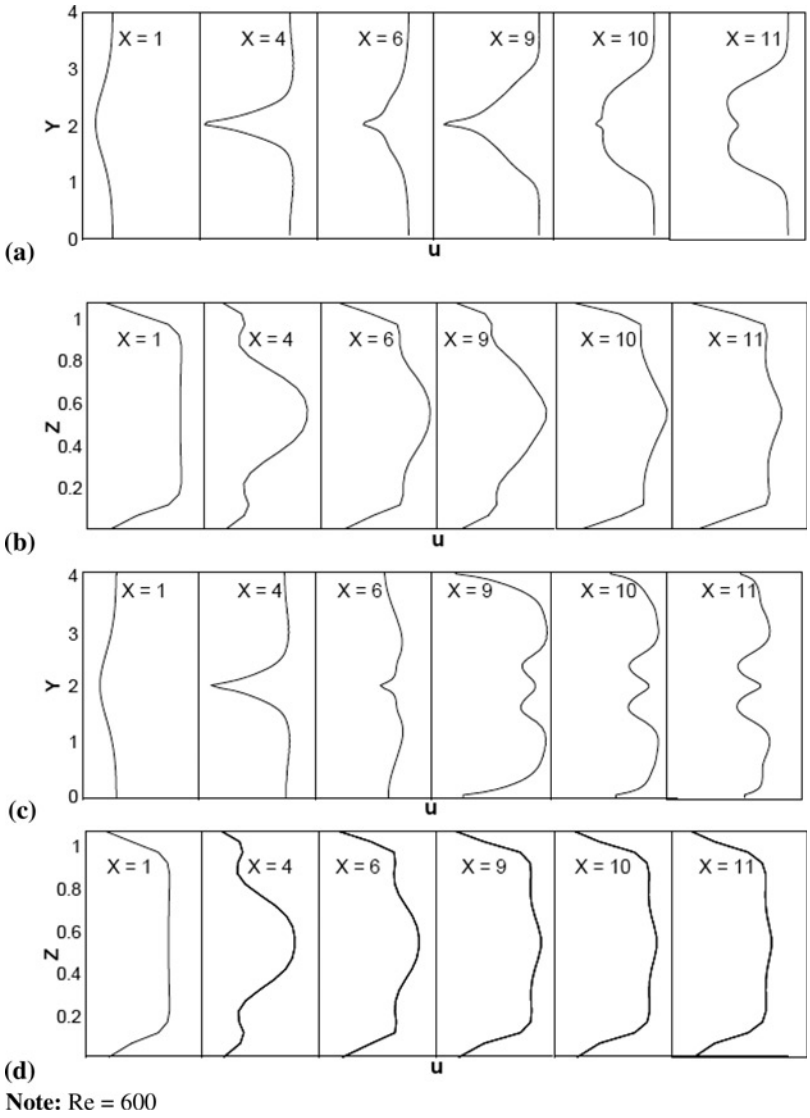

Figure 5.
u-velocity profiles for time-averaged field at different *X*-locations in (a) *X-Y* mid-plane; (b) *X-Z* mid-plane, for inline arrangement of tubes; (c) *X-Y* mid-plane and (d) *X-Z* mid-plane, for staggered arrangement of tubes

6.1.3 Streamline and temperature contour. Even though the velocity profiles at mid-plane shown above give an idea about development of the flow field downstream of the tubes, the actual flow behavior can be visualized with the help of streamlines in the cross-stream plane. Figures 7 and 8 present the streamline plots in the cross-stream plane at various streamwise locations ($X = 1.5$, 4.5, 5.75, 9.75 and 10.75) for inline and staggered arrangement of tubes, respectively. The location $X = 1.5$ considers the cross-stream plane ahead of the upstream tube and the locations $X = 4.5$ and 5.75 consider the cross-stream planes between the upstream and the downstream tubes. Comparison of cross-plane streamlines at locations $X = 1.5$ and 4.5 in Figures 7 and 8 shows nearly identical flow behavior as expected. In other words, there is no upstream effect of different tube

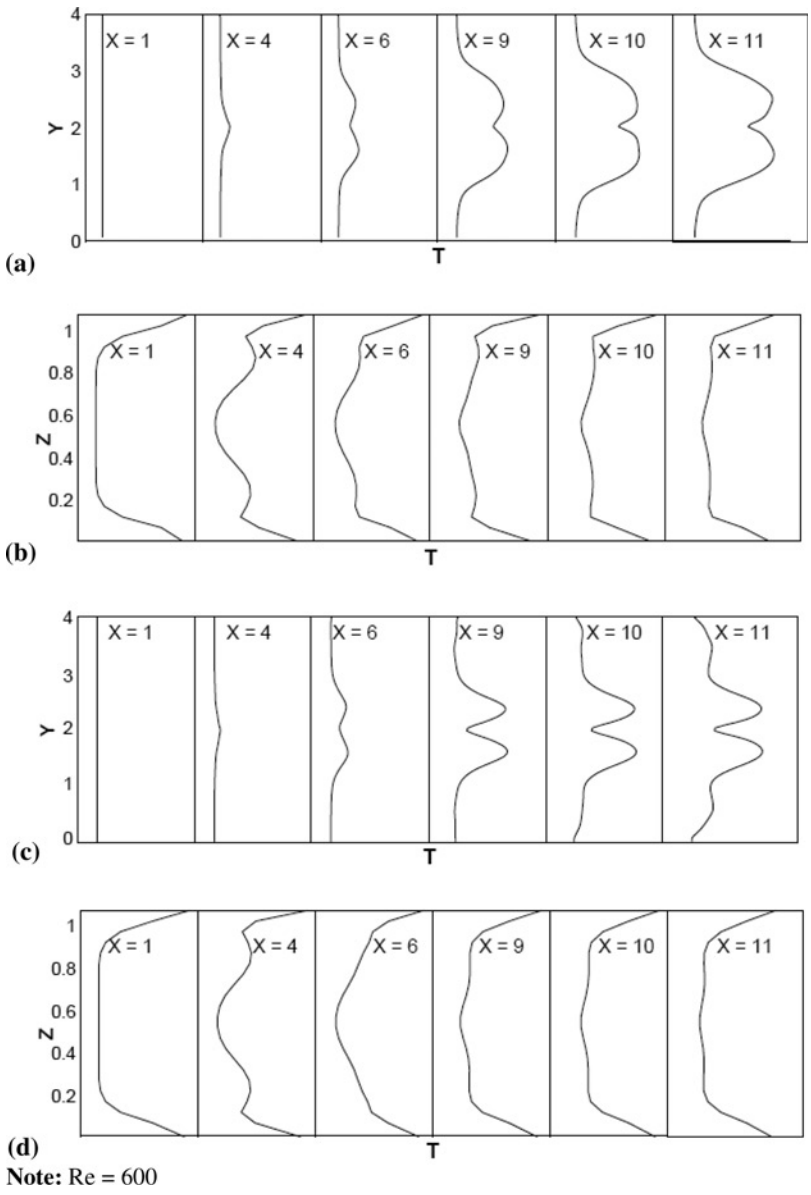

Figure 6.
Temperature profiles for time-averaged field at different X-locations in (a) X-Y mid-plane; (b) X-Z mid-plane, for inline arrangement of tubes; (c) X-Y mid-plane and (d) X-Z mid-plane, for staggered arrangement of tubes

arrangements. The locations $X = 9.75$ and 10.75 correspond to cross-stream planes behind the downstream tube. For these cross-stream plane locations, the nature of the longitudinal vortices behind the downstream tube show characteristic differences.

Figures 9(a) and (b) present the limiting streamlines and temperature contour plots, respectively, on the surfaces of upstream and downstream tubes for the inline arrangement of circular tubes. The qualitative nature of limiting streamline explains the behavior of flow separation and reattachment with respect to the tube surfaces. The

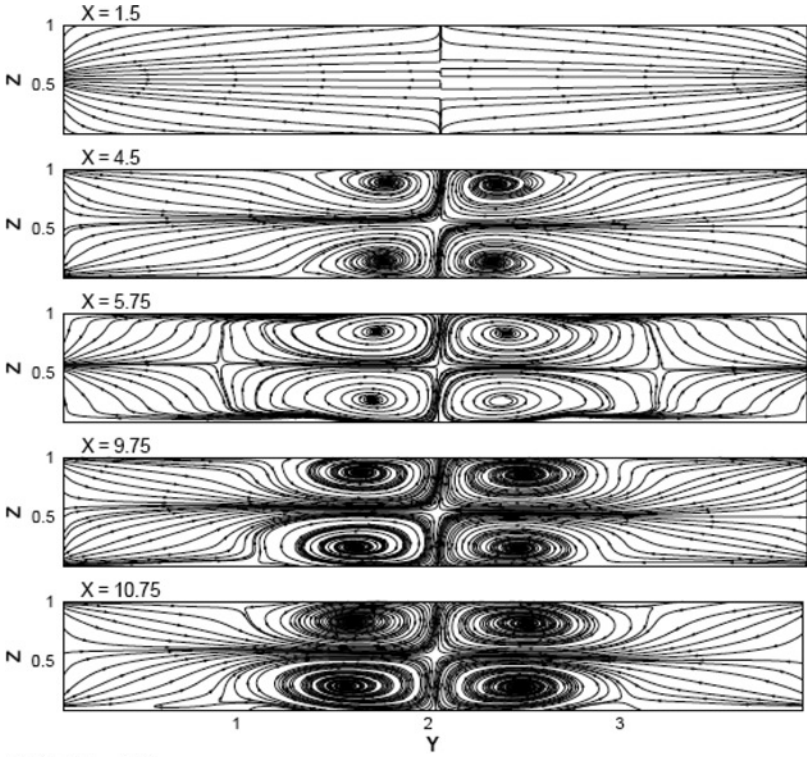

Note: Re = 600

Figure 7.
Cross-stream (*Y-Z*) streamline plots of time averaged field at different *X*-locations for inline arrangement of tubes

temperature contours on the upstream and downstream tube surfaces shown in Figure 9(b) indicate that the wake of the downstream tube has relatively lower bulk-mean temperature compared to that of the upstream tube. In other words, the heat transfer from the downstream tube surface is expected to be more compared to that from the upstream tube surface.

Figures 10(a) and (b) present the corresponding plots for the staggered tube arrangement. The limiting streamlines and temperature contours on the downstream half-tube surfaces are shown separately. The temperature contours from Figures 9(b) and 10(b) on the downstream tube surface(s) clearly indicate that the wake zone gets less heated for the staggered arrangement of tubes thereby heat transfer is expected to be relatively more in this case.

6.1.4 Span-averaged Nusselt number near bottom wall. The local Nusselt number near channel walls may be defined as:

$$Nu(x,y) = \frac{1}{1-\Theta_b}\left(-\frac{\partial\Theta}{\partial z}\right)_{z=0,H} \tag{4a}$$

In a similar way, the local Nusselt number on the tube surface can be written as:

$$Nu(x,y) = \frac{1}{1-\Theta_b}\left(-\frac{\partial\Theta}{\partial r}\right)_{r=R} \tag{4b}$$

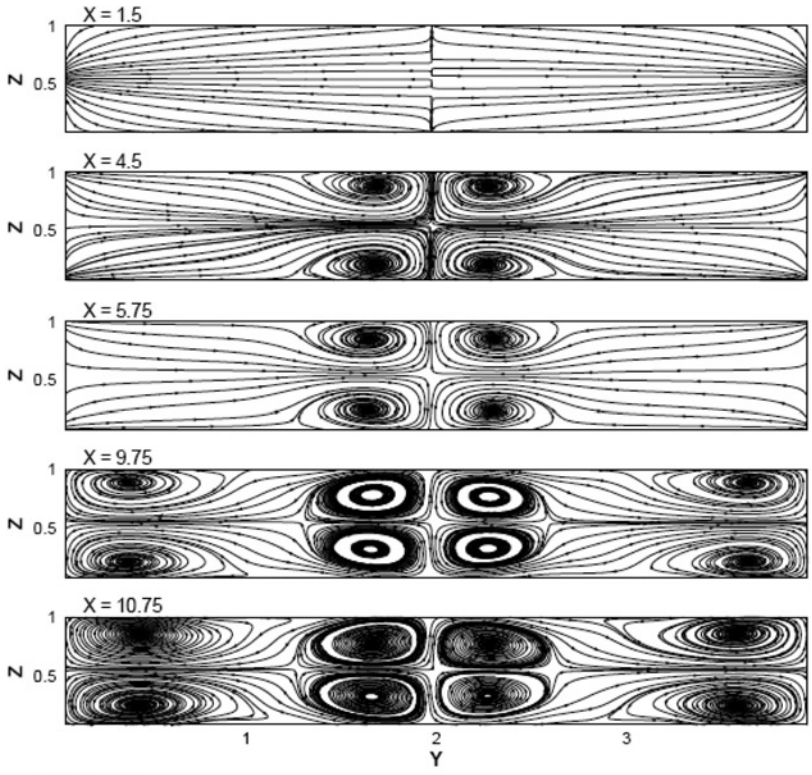

Figure 8.
Cross-stream (*Y-Z*) streamline plots of time-averaged field at different *X*-locations for staggered arrangement of tubes

Note: Re = 600

Here r is radial coordinate and is positive in outward direction of tube surface and R is radius of the tube. Also, Θ_b is the bulk-mean temperature of the fluid at a particular cross-stream location is defined as:

$$\Theta_b(x) = \frac{\iint_{A_c} \Theta_b(x,y,z)u(x,y,z)dA}{\iint_{A_c} u(x,y,z)dA} \tag{5}$$

where A_c is the area of cross-stream plane.
The span-averaged Nusselt number near the bottom wall at a particular cross-stream location becomes:

$$\overline{Nu}_{sp}(x) = \frac{1}{B}\int_0^B Nu(x,y)dy \tag{6}$$

where B is the width of the channel.

Figure 11(a) compares the variation of span-averaged Nusselt number along the length of the channel for inline and staggered arrangement of tubes. It is analogous to nature of variation of span-averaged convective heat transfer coefficient. It is observed that the Nusselt number till rear stagnation point of the upstream tube is almost same for both the arrangements beyond which the span-averaged Nusselt number for the staggered arrangement is slightly higher than that for inline arrangement. Figure 11(b)

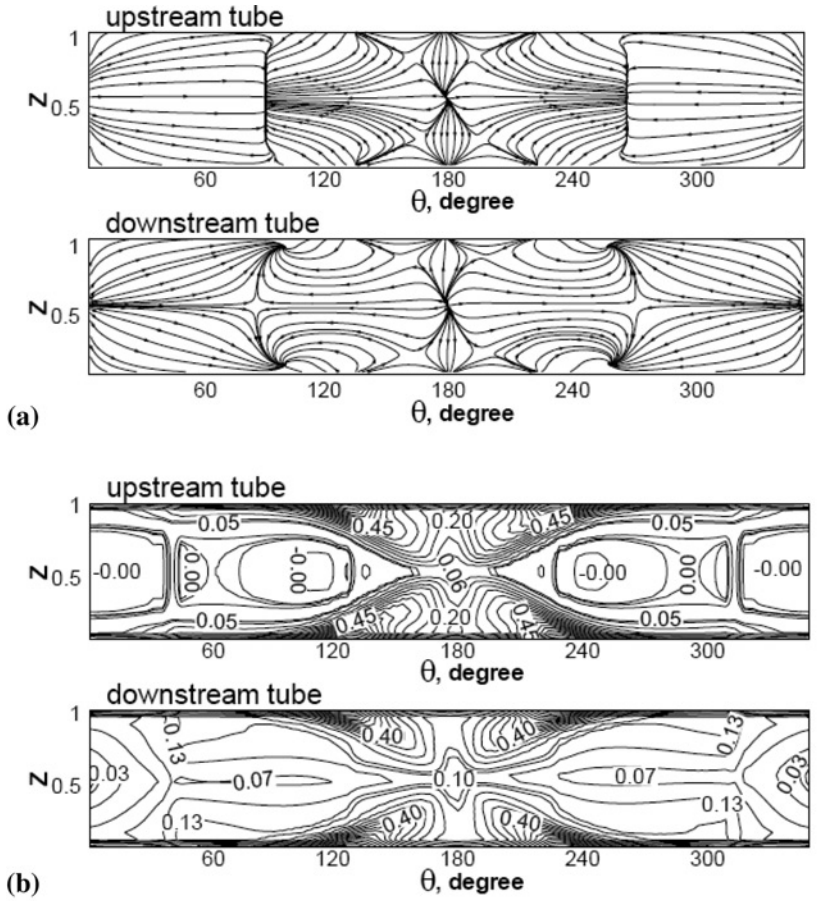

Notes: (a) Limiting streamlines near tube surfaces for inline arrangement of tubes; (b) temperature distribution near tube surfaces for inline arrangement of tubes; Re = 600

Figure 9.

compares variation of span-averaged pressure along the length of the channel. Variation of pressure has almost the same trend for both inline and staggered arrangement of tubes. The pressure drop appears due to presence of obstructions and solid walls in the flow field. Consequently, the location of the tubes plays a vital role in determining the pressure drop. The free passage in the downstream region for staggered arrangement of tubes offers less obstruction for the flow. Therefore, pressure drop for tubes in staggered arrangement is found to be less, compared to the inline arrangement of tubes.

6.1.5 Skin friction and Nusselt number near tube surfaces. Figures 12(a) and (b) present a comparison of height-averaged skin friction drag (Equation 7) and height-averaged Nusselt number (Equation 8) around the tube surfaces between the inline and staggered arrangement of tubes. The height-averaged skin-friction drag and height-averaged Nusselt number are defined as:

$$\bar{\tau}(\theta) = \frac{1}{H}\int \tau^*(\theta, z)\, dz \tag{7}$$

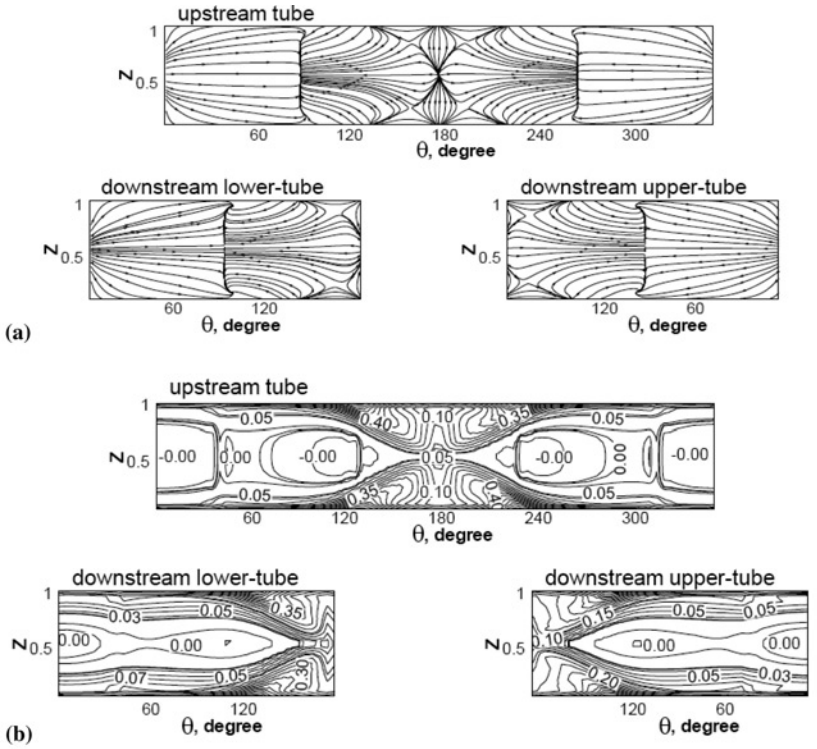

Figure 10.

Notes: (a) Limiting streamlines near tube surfaces for staggered arrangement of tubes; (b) temperature distribution near tube surfaces for staggered arrangement of tubes; Re = 600

where $\tau^* = (1/\mathrm{Re})(\partial u^*/\partial n^*)$ is the non-dimensionalized skin friction drag.

$$\overline{Nu}(\theta) = \frac{1}{H}\int_{\substack{\text{tube}\\ \text{surface}}} Nu(\theta, z)\, dz \tag{8}$$

The height-averaged skin friction drag around the tubes for both inline and staggered arrangements of tubes does not show significant differences except near the point of separation (Figure 12(a)). Moreover, the skin friction drag for the staggered downstream half-tubes is found to be smaller than that for the downstream inline tube. Figure 12(b) shows the height-averaged Nusselt number around the circumference of the tubes. In the inline arrangement of tubes, the downstream tube is in shadow of the upstream tube and so the fluid does not impinge on it directly. As a result, the Nusselt number near the forward stagnation region of the downstream tube is relatively lower. In the staggered arrangement of tubes, fluid impinges on the downstream tube almost without any obstruction, i.e. all the tubes in staggered arrangement are equally exposed to the flow. The upstream tubes for both the arrangements have almost similar variation of Nusselt number which shows that the upstream effect of downstream tubes is negligible.

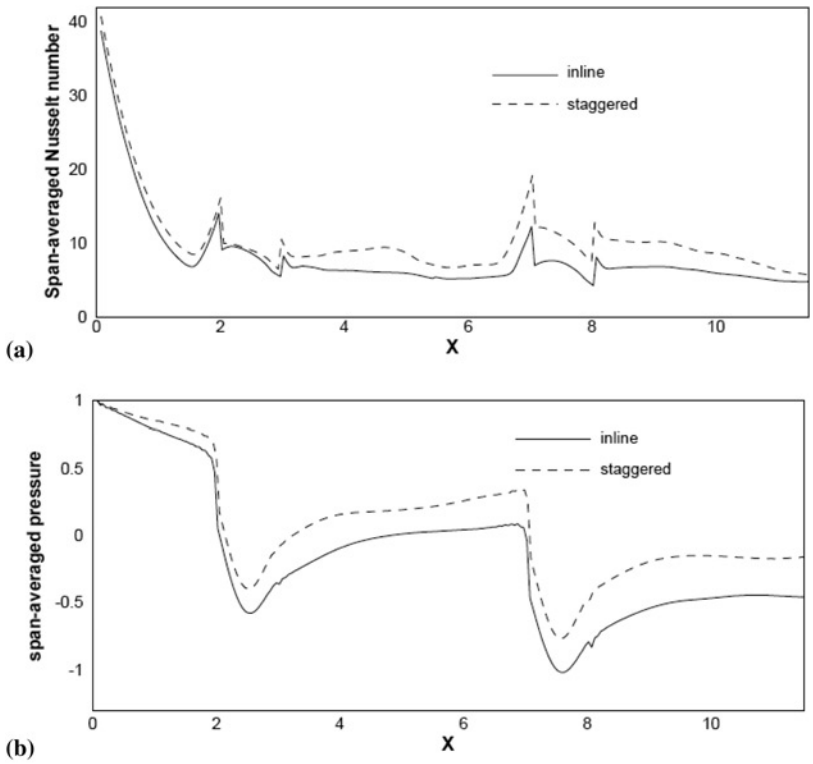

Notes: (a) Span-averaged Nusselt number variation near the bottom channel; (b) span-averaged pressure variation, along length of the channel; Re = 600

Figure 11.

6.2 Effect of Reynolds number and validation of computations

The effect of Reynolds number on heat transfer and pressure drop has been investigated for both the arrangements of tubes. A normalized estimate of heat transfer from the tube surfaces can be presented in terms of Colburn factor (j) defined as:

$$j = Nu/Re\,Pr^{0.33} \tag{9}$$

The dependence of j-factor on Reynolds number from the present computations for staggered arrangement of tubes in the bundle has been presented in Figure 13(a). The computed values of j-factor from the present study are compared with experimental results of Kwak *et al.* (2003) and with the correlation proposed by Rich (1973). A satisfactory agreement is observed between Rich's correlations and the present computations while the experimental results of Kwak *et al.* (2003) are seen to overestimate both the above results. This is primarily due to effect of confinement and also partly due to differing nature of inlet velocity profile. The ratio of channel height to tube diameter in present computations is 1.0 while that in the experimental results of Kwak *et al.* (2003) is 0.187. The correlations proposed by Rich (1973) hold for the channel confinement in the range of $0.16 < H/D < 1.29$. The present results show closer match than experimental results reported by Kwak *et al.* (2003) with correlations proposed by Rich (1973). Moreover, the inlet velocity profile in the present

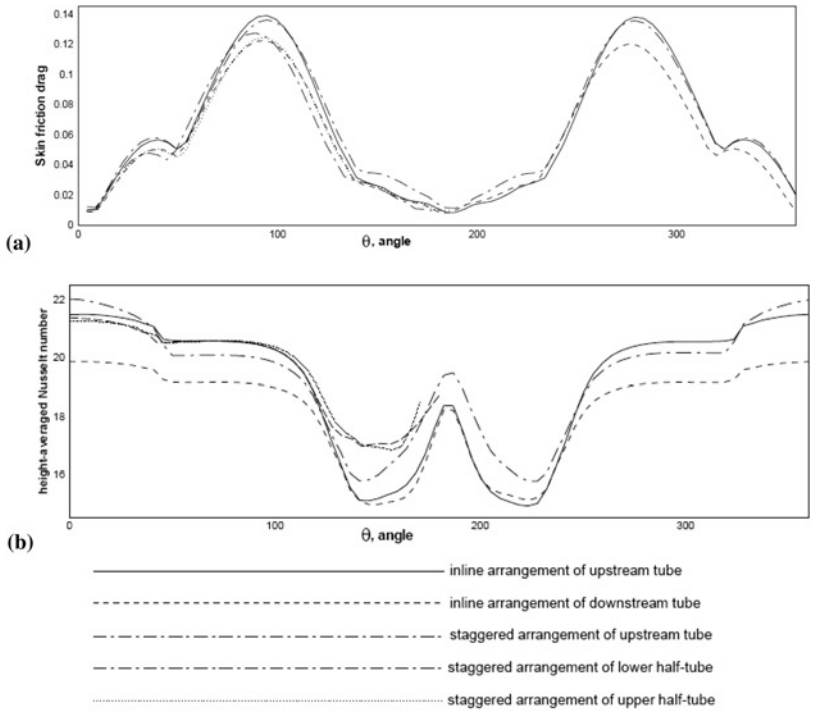

Figure 12.
Circumferential variation of height-averaged (a) skin friction and (b) Nusselt number for both inline and staggered arrangement of tubes

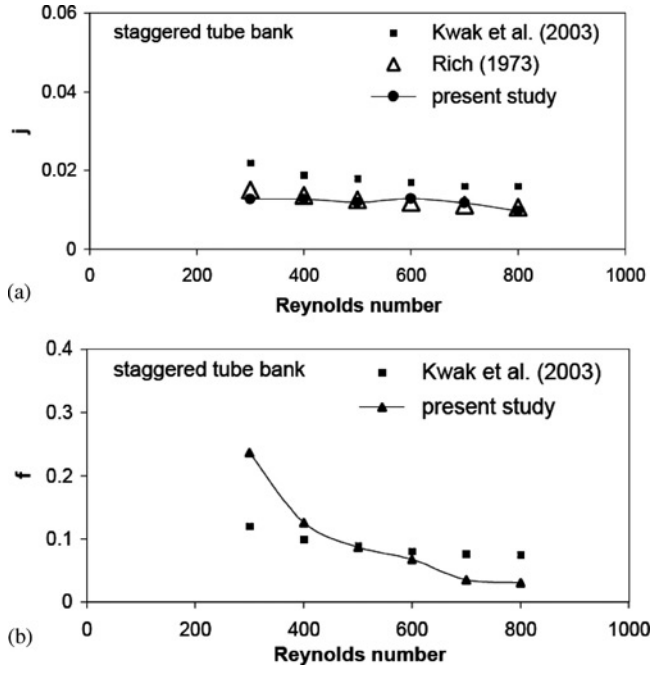

Figure 13.
Comparison of effect of Reynolds number for staggered arrangement of circular tubes upon (a) heat transfer (j-factor) and (b) friction factor (f-factor)

computations is of uniform type while for both the compared results it is fully developed. Figure 13(b) compares the variation of friction factor with Reynolds number against experimental results of Kwak *et al.* (2003) for staggered arrangement of circular tubes. The friction factor has been determined by using empirical correlations given by Kays and London (1964) for flow past unconfined tube banks.

$$f = \frac{2D}{4l_1}\left[\frac{\Delta p}{\rho U_m^2/2} - (K_c + K_e)\right]; \quad K_c = 0.42, K_e = -0.35 \tag{10}$$

It is important to note that the friction factor defined in Equation (10) gives direct information about the pressure drop, Δp, across the channel. The experimental results reported by Kwak *et al.* (2003) use the same correlations but due to their channel confinement being quite small as mentioned above and a fully developed flow entering the region, the wall shear stress is expected to show a weak dependence on Reynolds number. This is the main reason why the variation of friction factor presented in Figure 13(b) shows deviations from the results of Kwak *et al.* (2003). Even though the present results match well for Reynolds number in the range of 500-600, deviations are apparent for lower as well as higher Reynolds numbers.

6.3 Comparison of performance of inline and staggered arrangements of tubes

Figures 14(a) and (b) present dependence of *j*-factor and friction factor on Reynolds number for inline as well as staggered arrangement of tubes. In the low range of Reynolds number (Re < 450), inline arrangement of tubes possess better heat transfer behavior by causing smaller pressure drop as compared to staggered arrangement of tubes. As the Reynolds number increases, for inline arrangement of tubes, the wake zone widens and leads to reduction in heat transfer as shown in Figure 14(a). For staggered arrangement of tubes, the *j*-factor remains almost invariant with Reynolds number. Friction factor for both the arrangements in the considered range of Reynolds

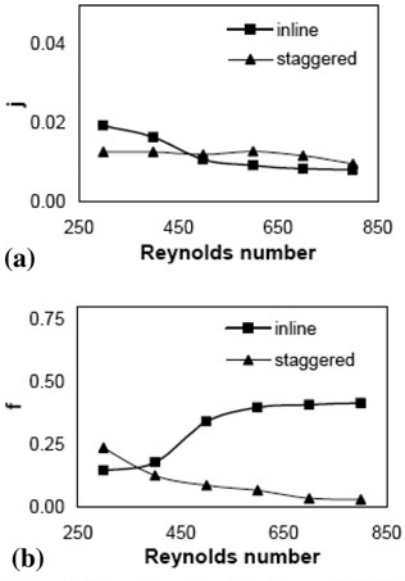

Notes: (a) Heat transfer, *j*-factor and (b) friction factor, *f*

Figure 14.
Comparison of inline and staggered arrangements of tubes for different Reynolds numbers

number has been compared for both the arrangements in Figure 14(b). The important observation made from results of Figures 14(a) and (b) is that for Re > 350, staggered arrangement of tubes are associated with higher heat transfer and smaller pressure drop. One of the effective ways to quantify the performance parameters for tube bundles in the considered arrangements is to consider the ratio of heat transfer and pressure drop for staggered and inline arrangement of tubes. The arrangement associated with higher heat transfer ratio (HTR) and smaller pressure drop ratio (PDR) will be preferred one. For a given Reynolds number, we define:

$$\text{Heat transfer ratio, HTR} = \frac{(\overline{N}u_o)_{\text{stag}}}{(\overline{N}u_o)_{\text{inl}}} \tag{11}$$

$$\text{Pressure drop ratio, PDR} = \frac{\Delta p_{\text{stag}}}{\Delta p_{\text{inl}}} \tag{12}$$

In Figures 15(a) and (b) HTR and PDR are presented to compare the performance of staggered and inline arrangement of tubes. It is evident from Figures 15(a) and (b) that for Re < 400, inline arrangement of tubes offers better performance than staggered arrangement of tubes. Further, for Re > 400, HTR gradually picks up and PDR decreases which is desirable. Hence, in situations where the objective is to enhance heat transfer without a stringent criterion being set on pressure drop, or the converse, a compromise is to be made to identify the range of Reynolds number associated with an optimum performance of the tube bundles for a particular arrangement.

7. Conclusions

A finite volume-based numerical investigation is carried out to study the flow and heat transfer for flow past inline and staggered arrangement of tube bundles confined in a rectangular channel. The investigations are performed after thorough grid-independence study and the computed results are validated against those available in literature. The present investigation identify the range of Reynolds number in which staggered arrangement of tubes in a tube bundle provide more heat transfer causing less pressure drop compared with inline arrangement of tubes. However, at lower Reynolds numbers inline arrangement of tubes are found to be preferable due to heat transfer and smaller pressure drop.

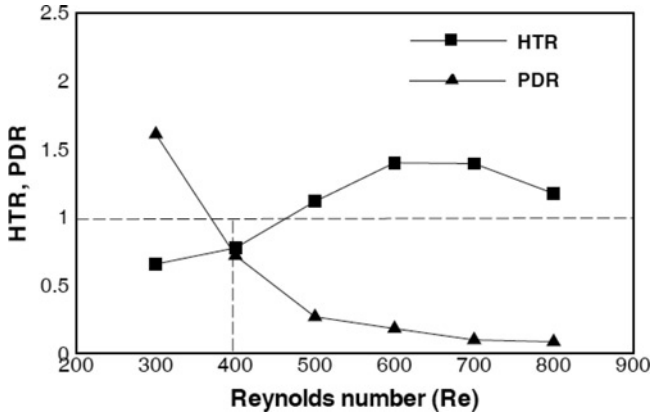

Figure 15.
Comparison of HTR and PDR of inline and staggered arrangements of tubes for different Reynolds numbers

References

Beal, S.B. and Spalding, D.B. (1999), "A numerical study of unsteady fluid flow in in-line and staggered tube banks", *Journal of Fluids and Structures*, Vol. 13, pp. 723-54.

Gangacharyulu, D. (2001), "Theoretical and experimental investigations on thermal performance analysis of cross flow compact heat exchangers", *International Journal of Heat Exchangers*, Vol. 1524-5608/2, pp. 201-18.

Herchang, Ay, Jiin, Y.J. and Jer-Nan, Y. (2002), "Local heat transfer measurements of plate finned-tube heat exchangers by infrared thermography", *International Journal of Heat and Mass Transfer*, Vol. 45, pp. 4069-78.

Kays, W.M. and London, A.L. (1964), *Compact Heat Exchangers*, 2nd ed., Ch. 5, McGraw-Hill, New York, NY.

Khan, W.A., Culam, J.R. and Yovanovich, M.M. (2006), "Convection heat transfer from tube banks in crossflow: analytical approach", *International Journal of Heat and Mass Transfer*, Vol. 49 Nos. 25/26, pp. 4831-8.

Kim, Y. and Kim, Y. (2005), "Heat transfer characteristics of flat plate finned-tube heat exchangers with large fin pitch", *International Journal of Refrigeration*, Vol. 28, pp. 851-8.

Kwak, K.M., Torii, K. and Nishino, K. (2003), "Heat transfer and pressure loss penalty for the number of tube rows of staggered finned-tube bundles with a single transverse row of winglets", *International Journal of Heat and Mass Transfer*, Vol. 46 No. 1, pp. 175-80.

Leonard, B.P. (1979), "A stable and accurate convective modeling procedure based on quadratic upstream interpolation", *Computational Methods Applied Mechanical Engineering*, Vol. 19, pp. 59-98.

Liu, X.L., Tao, W.Q. and He, Y.L. (2005), "A simple method for improving the SIMPLER algorithm for numerical simulations of incompressible fluid flow and heat transfer problems", *Engineering Computations: International Journal for Computer-Aided Engineering and Software*, Vol. 22 No. 8, pp. 921-39.

Orlanski, I. (1976), "A simple boundary condition for unbounded flows", *Journal of Computational Physics*, Vol. 21, pp. 251-69.

Patankar, S.V. (1980), *Numerical Heat Transfer and Fluid Flow*, Hemisphere, Washington, DC.

Ramezanpour, A., Iraj, M., Ramin, R. and Hassan, S. (2006), "Numerical study of staggered tube bundle in turbulent cross flow for an optimum arrangement", *International Journal of Heat Exchangers*, Vol. 1524-5608/7, pp. 37-56.

Rich, D.G. (1973), "The effect of fin spacing on the heat transfer and friction performance of multi-row smooth plate fin-and-tube heat exchanger", *ASHRAE Transactions*, Vol. 79 No. 2, pp. 137-45.

Tiwari, S., Biswas, G., Prasad, P.L.N. and Sudipta, B. (2003), "Numerical prediction of flow and heat transfer in a rectangular channel with a built-in circular tube", *Journal of Heat Transfer (ASME)*, Vol. 125, pp. 413-21.

Tony Sheu, W.H. and Tasi, S.F. (1999), "A comparison study on fin surfaces in finned-tube heat exchangers", *International Journal of Numerical Methods for Heat and Fluid Flow*, Vol. 9 No. 1, pp. 92-106.

Wilson Safwat, A. and Bassiouny Khalil, M. (2000), "Modeling of heat transfer for flow across tube banks", *Chemical Engineering and Processing*, Vol. 39, pp. 1-14.

Corresponding author
Shaligram Tiwari can be contacted at: shaligt@iitm.ac.in